nature communications

Article

https://doi.org/10.1038/s41467-023-36653-3

Inducing transient enantiomeric excess in a molecular quantum racemic mixture with microwave fields

Received: 23 June 2022

Accepted: 10 February 2023

Published online: 20 February 2023

Check for updates

Wenhao Sun[1,2], Denis S. Tikhonov[1,2], Himanshi Singh[1,2], Amanda L. Steber[1,2,3], Cristóbal Pérez[1,2,3] & Melanie Schnell[1,2] ✉

Chiral molecules with low enantiomer interconversion barriers racemize even at cryogenic temperatures due to quantum tunneling, forming a racemic mixture that is impossible to separate using conventional chemical methods. Here we both experimentally and theoretically demonstrate a method to create and probe a state-specific enantiomeric enrichment for such molecular systems. The coherent, non-linear, and resonant approach is based on a microwave six-wave mixing scheme and consists of five phase-controlled microwave pulses. The first three pulses induce a chiral wavepacket in a chosen rotational state, while the consecutive two pulses induce a polarization for a particular rotational transition (listen transition) with a magnitude proportional to the enantiomeric excess created. The experiments are performed with the transiently chiral molecule benzyl alcohol, where a chiral molecular response was successfully obtained. This signal demonstrates that enantiomeric excess can be induced in a quantum racemic mixture of a transiently chiral molecule using the developed microwave six-wave mixing scheme, which is an important step towards controlling non-rigid chiral molecular systems.

Chirality is an ubiquitous and fundamental phenomenon in nature. A chiral molecule has a pair of enantiomers, which are non-superimposable mirror images of each other. They share almost all physical properties, but often possess distinct functionality in chemical reactions and biological activity with chiral environments. For instance, enantiomers of chiral drugs often exhibit different effectiveness and toxicity[1]. As molecular chirality plays an essential role in many fundamental aspects of physics, chemistry, and biology, great efforts have been made to characterize, differentiate, and manipulate chiral molecules. Besides the traditional methods in chemistry, such as chromatography[2] and capillary electrophoresis[3], various chiroptical techniques using circularly polarized radiation have been developed to determine the absolute configuration and enantiomeric excess (ee) of a chiral sample, such as vibrational circular dichroism (VCD)[4,5] and photoelectron circular dichroism (PECD)[6,7]. Recently, the microwave three-wave mixing (M3WM) approach, which is a resonant, coherent, and non-linear spectroscopic technique, became a new methodology for chiral differentiation and quantification[8,9]. The chiral sensitivity arises from the mirror symmetry of the electronic structures of enantiomers, making the triple products of their three electric dipole-moment components ($\boldsymbol{\mu}_a \cdot [\boldsymbol{\mu}_b \times \boldsymbol{\mu}_c]$) equal in magnitude but opposite in sign, which can be interrogated using a combination of selected rotational transitions.

In addition to chiral analysis, the M3WM technique showcased its capability to achieve chiral separation at the molecular level[10–13]. Through the interference between the chiral sensitive M3WM path and a direct excitation path, enantiomers can be selectively enriched in chosen rotational states. As the sample is studied in the gas phase with

---

[1] Deutsches Elektronen-Synchrotron DESY, Notkestr. 85, 22607 Hamburg, Germany. [2] Institute of Physical Chemistry, Christian-Albrechts-Universität zu Kiel, Max-Eyth-Str. 1, 24118 Kiel, Germany. [3] Present address: Departamento de Química Física y Química Inorgánica, Facultad de Ciencias-I.U. CINQUIMA, Universidad de Valladolid, E-47011 Valladolid, Spain. ✉ e-mail: melanie.schnell@desy.de

cold molecular sources (e.g. buffer-gas cooling and supersonic jets), this technique can be applied not only to molecules with permanent chirality, such as 1,2-propanediol[10] and carvone[11] but also to molecules that exhibit transient chirality, such as cyclohexylmethanol (CHM)[12], which are impossible to separate via conventional separation techniques, such as chromatography. However, when it comes to molecules that can interconvert their handedness via quantum tunneling through a large-amplitude motion (LAM), the enantiomers can no longer be isolated in a cold supersonic jet, where the molecules are cooled to a rotational temperature (T_{rot}) of a few Kelvin[14]. The sample naturally appears as a racemic mixture during the jet expansion. These molecules have two (or more) minima on the potential energy surface. Each minimum corresponds to a certain enantiomer, separated by an achiral transition state (Fig. 1). The stationary states of such molecules are of a specific parity with respect to the inversion operation that we will denote as $|\pm\rangle$. They are the positive and negative combinations of the non-stationary localized wavepackets with a chosen parity ($|\pm\rangle = \frac{1}{\sqrt{2}}(|R\rangle \pm |S\rangle)$). A specific enantiomeric state of such a molecule thus can be achieved by generating a coherent superposition of the states $|\pm\rangle$ with opposite parity[15–18]. Such an approach has been proposed for rotational states of asymmetric rotors[19,20]; however, to date, no experimental demonstration has been reported.

Herein, we present both theoretical and experimental demonstration of inducing enantiomeric excess from a racemic mixture of a transiently chiral molecule, benzyl alcohol (BA), in the gas phase. This molecule undergoes a LAM, corresponding to a concerted rotation of the CH_2OH and OH groups in the plane above the phenyl ring. This tunneling motion with a barrier of about 280 cm^{-1} transfers one enantiomer into the other one (see Fig. 1)[21]. It changes the sign of the electric dipole-moment component along the b-axis in the inertial principal axis system (PAS). The corresponding b-type rotational transitions occur between the two tunneling states of opposite symmetry. Because of these interstate transitions, both microwave three-wave mixing[8,22–24] and the related microwave population transfer schemes become impossible[10,11,22], as three rotational transitions cannot form a closed cycle due to symmetry considerations. Instead, five resonant excitation pulses are needed to induce the chiral response in the form of a "listen" transition in a suitable system of six rotational levels (see Fig. 1). This chiral response is not directly excited, and its amplitude is dependent on the enantiomeric excess of the sample. By detecting a listen (L) signal with non-zero intensity, we demonstrate that this microwave six-wave mixing (M6WM) scheme is feasible to create a transiently chiral ensemble of BA molecules in the rotational state of interest, despite a fast interconversion of the two enantiomers via the tunneling motion. In the following, we first provide the theoretical derivation of the M6WM scheme, followed by the experimental implementation and demonstration.

Results

Principle of the M6WM approach

We will start with an introduction of the M6WM scheme, which consists of five sequential resonant pulses. They correspond to a closed loop of six transitions that connect six states ($J^{\pm}_{K_aK_c}$) in the following sequence: $|1^-_{01}\rangle \to |2^-_{11}\rangle \to |2^+_{02}\rangle \to |1^+_{01}\rangle \to |2^+_{11}\rangle \to |2^-_{02}\rangle$, as illustrated in Fig. 1. Here, $J_{K_aK_c}$ denote the asymmetric rotor rotational state with J being the total angular momentum quantum number, K_a/K_c being the projections of this momentum onto the a-/c- principal axes of the molecule, respectively, and ± indicating the parity of the torsional state of the molecule. For a theoretical description, the sequence of pulses is treated as a set of subsequent two-level Rabi oscillations (a detailed derivation is given in the Supplementary Information). After applying the five excitation pulses, a macroscopic polarization **P**, which oscillates with amplitude A at the frequency of the $|2^-_{02}\rangle \to |1^-_{01}\rangle$ listen transition (ν_{L}), is coherently induced:

$$\mathbf{P}_{2^-_{02}\to 1^-_{01}} \propto \overbrace{-\boldsymbol{\mu}_{2^-_{02}\to 1^-_{01}} \cdot \sin(\Omega_1\tau_1) \cdot \left(\prod_{k=2}^{5} \sin\left(\frac{\Omega_k\tau_k}{2}\right)\right)}^{\propto A} \cdot \sin\left(2\pi\nu_{\mathrm{L}}t - \Phi + \sum_{k=1}^{5} s_k\varphi_k\right). \tag{1}$$

where $\boldsymbol{\mu}_{2^-_{02}\to 1^-_{01}}$ is the transition dipole moment for the induced listen transition $|2^-_{02}\rangle \to |1^-_{01}\rangle$, $\Omega_k = \frac{\boldsymbol{\mu}_k\mathbf{E}_k}{\hbar}$ is the Rabi frequency of the k-th pulse in the M6WM sequence, where the vector $\mathbf{E}_k$ describes its field strength and polarization direction, and $\boldsymbol{\mu}_k$ denotes the transition dipole moment of the transition induced with it[25,26], τ_k and φ_k are the pulse duration and phase, and Φ is the starting phase of the listen signal.

Equation (1) demonstrates the optimal conditions for the observation of the coherently induced polarization $\mathbf{P}_{2^-_{02}\to 1^-_{01}}$, the amplitude of which depends on the Rabi frequency. The first pulse is resonant to the $|1^-_{01}\rangle \leftrightarrow |2^-_{11}\rangle$ intrastate transition. This pulse should be a $\pi/2$-pulse ($\Omega_1\tau_1 = \pi/2$), which drives the population difference between the $|1^-_{01}\rangle$ and $|2^-_{11}\rangle$ rotational states into coherence. The other four pulses transfer this coherence to the final state $|2^-_{02}\rangle$ via the pathway $|2^-_{11}\rangle \to |2^+_{02}\rangle \to |1^+_{01}\rangle \to |2^+_{11}\rangle \to |2^-_{02}\rangle$, and they should be π-pulses ($\Omega_k\tau_k = \pi$ for $k = 2, \ldots, 5$). As a result, a final coherence at the listen

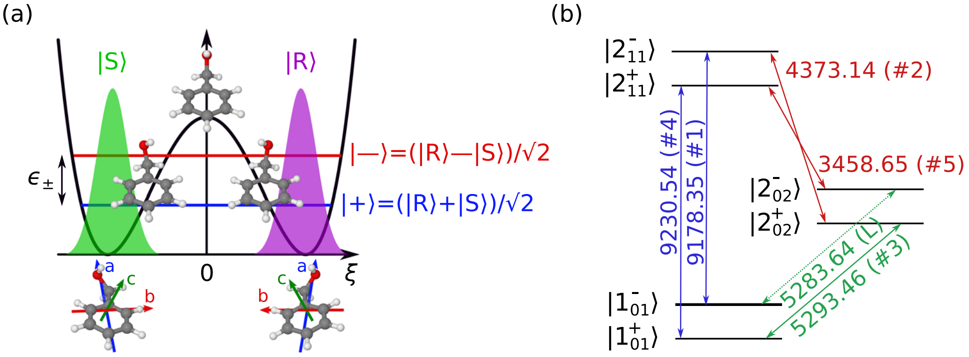

Fig. 1 | Double-well potential and rotational level scheme. a Schematic representation of the enantiomer interconversion mechanism in benzyl alcohol (BA). The $|\pm\rangle$ states denote the vibronic ground state with opposite parity. The $|R\rangle$ and $|S\rangle$ states represent the localized wavepackets of a particular chirality. ξ is the large amplitude motion coordinate. $\epsilon_{\pm}$ corresponds to the energy difference between the two tunneling states, which is experimentally determined to be 492.816(2) MHz for BA arising from a barrier with a height of about 280 cm^{-1}[21]. **b** Rotational level scheme of BA used in our experiment. Each rotational level is marked as $J^{\pm}_{K_aK_c}$, where J is the total angular momentum, K_a and K_c are the projections of the angular momentum onto the molecular axes a and c, and ± indicates the parity of the torsional state. M sublevels of the rotational states are omitted here for clarity[29]. The arrows indicate the transitions involved. Each transition is labeled with its frequency (in MHz) and its order in the sequence of the pulses (in parentheses). "L" indicates the "listen" transition, which is not directly excited by the pulse scheme but coherently induced.

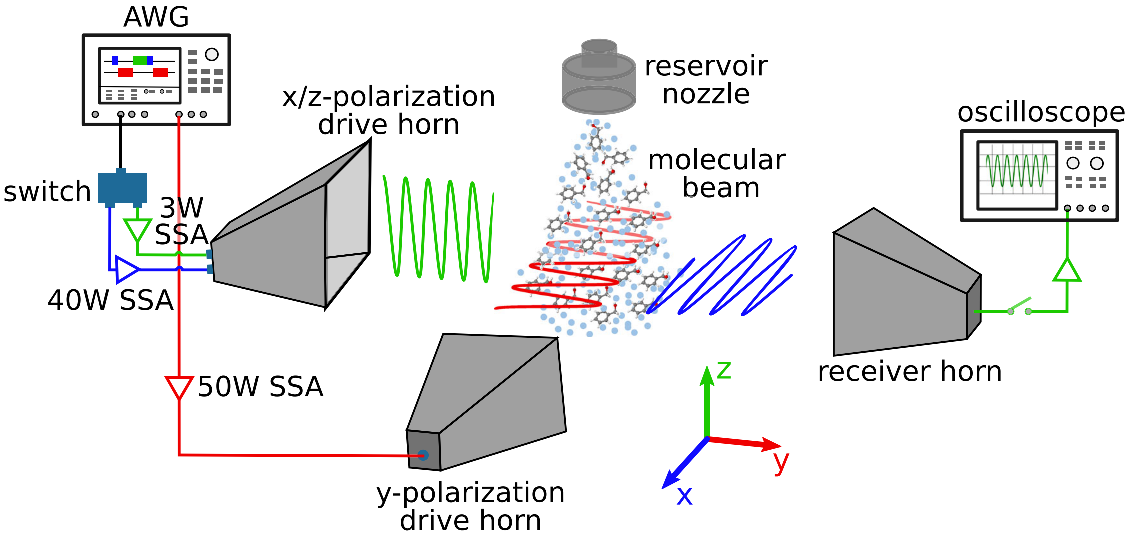

Fig. 2 | Schematic diagram of the state-specific enantiomeric enrichment experiment. The BA molecular sample seeded in neon with a stagnation pressure of about 3 bar is supersonically expanded into a vacuum chamber via a solenoid valve pulsing at 6 Hz. Five excitation pulses are generated from the two channels of the arbitrary waveform generator (AWG). The pulse sequence from channel 1 (CH1) is fed through the designated outputs of a single-pole-double-throw (SPDT) switch. Blue, red, and green colors represent the polarization directions of the microwave fields in the laboratory frame, which match the color code in the rotational level scheme as provided in Fig. 1. Each branch is equipped with a solid-state amplifier (SSA). The amplified microwave pulses are sequentially broadcast in the designated polarization directions to interact with the molecular jet using two dual-polarization horn antennae. The free induction decay (FID) of the resulting molecular response is collected in the z-polarization direction by a receiver horn and averaged by a fast digital oscilloscope.

transition is obtained with a maximum amplitude (A), when $\Omega_k \tau_k$ equals to $\pi/2$ for pulse #1, and π for pulse #2 – #5. The directions of the transition dipole moments (a-/b-/c-types are mutually orthogonal) also provide the required polarization directions of the pulses. There are three groups of pulses that need to be orthogonal to each other: pulses #1 and #4, pulses #2 and #5, and pulse #3, which is also indicated by the color scheme in Fig. 1b. The latter pulse (#3) should have the same polarization as the listen transition that is being collected.

The absolute phase of $\mathbf{P}_{2_{02}^{-}\to 1_{01}^{-}}$ depends on specific aspects of the experimental setup, such as the durations and phases of the five excitation pulses, delays between them, and cable lengths[27]. When the phase of pulse #k (φ_k) is varied, the phase of $\mathbf{P}_{2_{02}^{-}\to 1_{01}^{-}}$ changes accordingly, with a linear factor $s_k = \pm 1$. The factor s_k equals +1, when the transition goes up in energy ($k = 1, 4$), or equals −1, when the transition goes down in energy ($k = 2, 3, 5$), as described in more detail in the Supplementary Information.

M6WM spectroscopy

The experiment was carried out using a modified broadband Fourier transform microwave spectrometer, as shown schematically in Fig. 2. The molecular sample of BA was introduced into the vacuum chamber via supersonic jet expansions using neon as carrier gas. In the jet, the molecules were rapidly cooled to a T_{rot} of ~1–2 K via BA-neon collisions so that a substantial population difference was generated in the rotational states of interest. The ensemble of molecules was sequentially polarized with the five microwave pulses. In order to spatially broadcast the pulses in three mutually orthogonal planes, two dual-polarization horn antennae were installed at 90° in the vacuum chamber. After polarization, the decay of the induced macroscopic polarization at ν_{L} was received by a third horn on the detection side, digitized, and averaged on a fast digital oscilloscope.

Prior to the M6WM experiments, the pulse durations for the $\pi/2$ or π conditions were determined for each pulse by measuring the corresponding nutation curve. The collected nutation curves are provided in the Supplementary Section 2.2, and the optimized pulse sequence is presented in Fig. 3a. The determined pulse durations are approximate to the effective $\pi/2$ or π conditions averaged over M subsets of the rotational states[28–30]. Afterwards, we performed a series of M6WM experiments, in which the phase of one excitation pulse (φ_k) was systematically varied at a time in steps of 18° from 0° to 360° to evaluate the phase behavior of the M6WM signal at ν_{L}. The other remaining four pulses were kept unchanged in the scans. At each phase being scanned, 20,000 FIDs were collected and averaged at the frequency of the listen transition, $\nu_{\mathrm{L}} = 5283.64$ MHz. Each scan was carried out repeatedly five times, allowing us to assess the repeatability of the observations. The results are summarized in Fig. 3b.

Analysis of the M6WM signal

According to Eq. (1), the molecular response induced from the M6WM cycle, S_{M6WM}, at the frequency ν_{L} of the listen transition $2_{02}^{-} - 1_{01}^{-}$, should have a constant amplitude (A_{M6WM}) over the five sets of scans, and its phase (φ_{M6WM}) should be correlated with the phases of the five pulses. In each scan, the phase of one pulse (φ) was varied from 0° to 360°, whereas the phase of the other four pulses remained fixed. The induced polarizations can, thus, be expressed as $A_{\mathrm{M6WM}} \sin(2\pi\nu_{\mathrm{L}} t - \Phi' + s_k \varphi_k)$, where Φ' combines the starting phase Φ in Eq. (1) and the phases of the phase-invariant pulses in the pulse sequence. Hence, S_{M6WM} should have a linear phase dependence on φ_k with the coefficient s_k. In scans #1 and #4, $s_k = +1$; in scans #2, #3, and #5, $s_k = -1$. However, as shown in Fig. 3b, the observations in the experiments exhibit unanticipated phase dependence patterns. The signal intensities at ν_{L} are not constant, and the phases are not linearly correlated with φ_k.

With careful examinations that are described in the Supplementary Section 2.4, we analyzed that the observed signal at ν_{L} was a result of the interference between the expected S_{M6WM} signal and perturbation signals at ν_{L} (S_{c2} and S_{c3}) when applying pulses #2 and #3. The presence of S_{c2} and S_{c3} is presumably attributed to off-resonance excitations due to the power leakage in the electronic circuit. The two perturbation signals had constant amplitudes (A_{c2} and A_{c3}) throughout the experiments, and their phases (φ_{c2} and φ_{c3}) were positively and linearly dependent on the phase of pulses #2 and #3, respectively, as shown in Supplementary Figs. 18 and 19 in the Supplementary

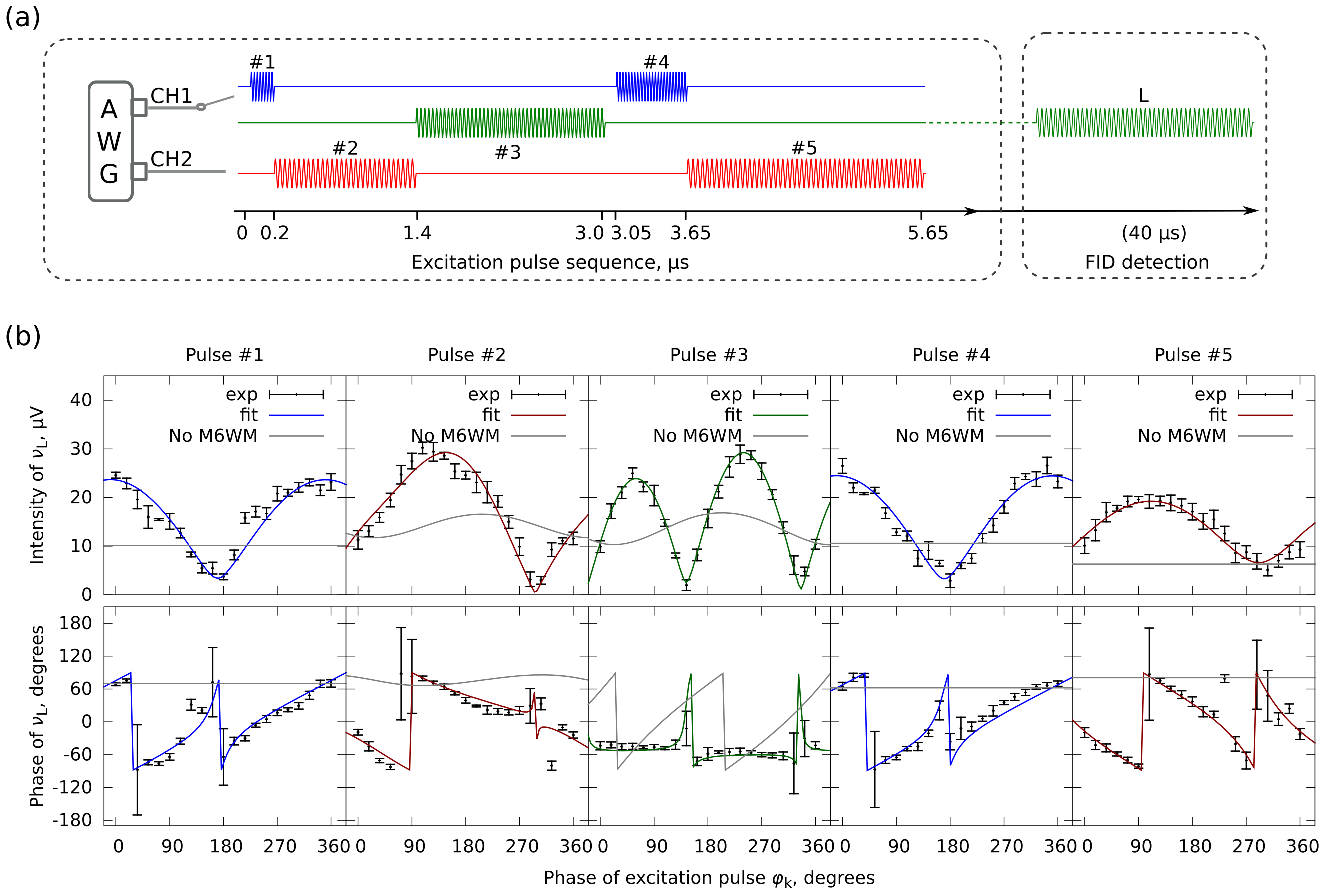

Fig. 3 | M6WM spectroscopy of BA. a The experimental M6WM pulse sequence, where the colors of the microwave pulses match the laboratory frame as in Fig. 2. The durations correspond to an optimized $\pi/2$-pulse for pulse #1 and π-pulses for pulses #2 – #5. 40 µs of FID for the frequency of the listen transition (ν_L) was recorded after the five excitation pulses, the duration of which is not to scale. **b** The resulting phase dependence patterns in amplitude (top) and phase (bottom) at the listen transition (ν_L). They were obtained by individually scanning the phases of the corresponding pulses (φ_k) and measuring the respective amplitude and phase of ν_L at 5283.64 MHz. Here, "phase of ν_L" denotes the arctangent of the tangent of the phase. The experimental results are represented in black with error bars. The errors are calculated from a set of five repeated measurements, in which each phase point was an average of 20,000 FIDs. In the least-squares fits, the amplitudes and the phases (in tangent) are fitted simultaneously. The overall fit for each set is represented in the color that matches the polarization of the corresponding microwave pulse whose phase was varied in the experiment. The gray line in each panel is the simulated amplitude or phase by excluding the M6WM component from the complete fit as discussed in the main text.

Information. The phase dependence coefficients of φ_{c2} and φ_{c3} are denoted as s_{c2} and s_{c3}. In scan #2, where the phase of pulse #2 (φ_2) was scanned, φ_{c2} positively and linearly varied with φ_2, while φ_{c3} was independent of φ_2. Therefore, $s_{c2} = +1$, and $s_{c3} = 0$. Likewise, φ_{c3} changed along with φ_3 in scan #3 and $s_{c3} = +1$, whereas φ_{c2} did not ($s_{c2} = 0$). In the other three scans, both φ_{c2} and φ_{c3} remained constant ($s_{c2} = 0$, and $s_{c3} = 0$), as φ_2 and φ_3 were not varied. With a clear understanding of the different phase dependencies of φ_{c2}, φ_{c3}, and φ_{M6WM}, we were able to perform a least-squares fit on each set of the scan to decompose the observed pattern and extract the S_{M6WM} signal. The molecular response from each scan is fitted independently as a sum of the individual interfering signals, where the total listen signal amplitude (A) and the total phase (Φ) are given by the following expressions:

$$\begin{cases} A^2 = \sum_{m=1}^{N}\sum_{n=1}^{N} A_m A_n \cos(s_m\varphi_k + \phi_m - s_n\varphi_k - \phi_n) \\ \tan(\Phi) = \dfrac{\sum_{m=1}^{N} A_m \sin(s_m\varphi_k + \phi_m)}{\sum_{m=1}^{N} A_m \cos(s_m\varphi_k + \phi_m)} \end{cases} . \tag{2}$$

Here, N is the number of interfering signals, φ_k is the scanned phase, A_m, A_n, ϕ_m, and ϕ_n are the amplitudes and the starting phases of the individual components, which are fitted to the observed experimental signals, s_m and s_n are the associated phase dependence coefficients. The square of the listen signal amplitude (A^2) and the tangent of the listen signal phase ($\tan(\Phi)$) are fitted simultaneously. The details on the procedure and the scripts used for the fitting are given in the Supplementary Information.

As in scans #2 and #3, the phases of all three interfering components have different phase dependencies on φ_k (i.e., in scan #2: $s_{c2} = +1$, $s_{c3} = 0$, and $s_2 = -1$; in scan #3: $s_{c2} = 0$, $s_{c3} = +1$, and $s_3 = -1$), they can be explicitly separated in the fit, as shown in Fig. 4. However, in the other three scans (#1, #4, and #5), as both S_{c2} and S_{c3} are phase-invariant, these two co-excited signals cannot be meaningfully separated. The sum of them is fitted as one phase-invariant signal instead. In each scan, the least-squares fit is obtained over the five repeats, and the experimental uncertainty is derived at each phase point as well. The fit results are summarized in Table 1 and are presented in Fig. 3b together with the experimental observations. The signal component with the anticipated phase dependence is assigned to S_{M6WM}, and it has a consistently constant amplitude of 13–14 µV throughout the five scans, clearly demonstrating the feasibility of the approach. In Fig. 3b, the curves based on the complete least-squares fits are represented using colored lines, while the simulations of the sum of S_{c2} and S_{c3} are plotted with gray lines, where the M6WM components are excluded. In this manner, the signal patterns with and without the presence of S_{M6WM} are revealed, and detailed demonstrations are further provided in Fig. 4.

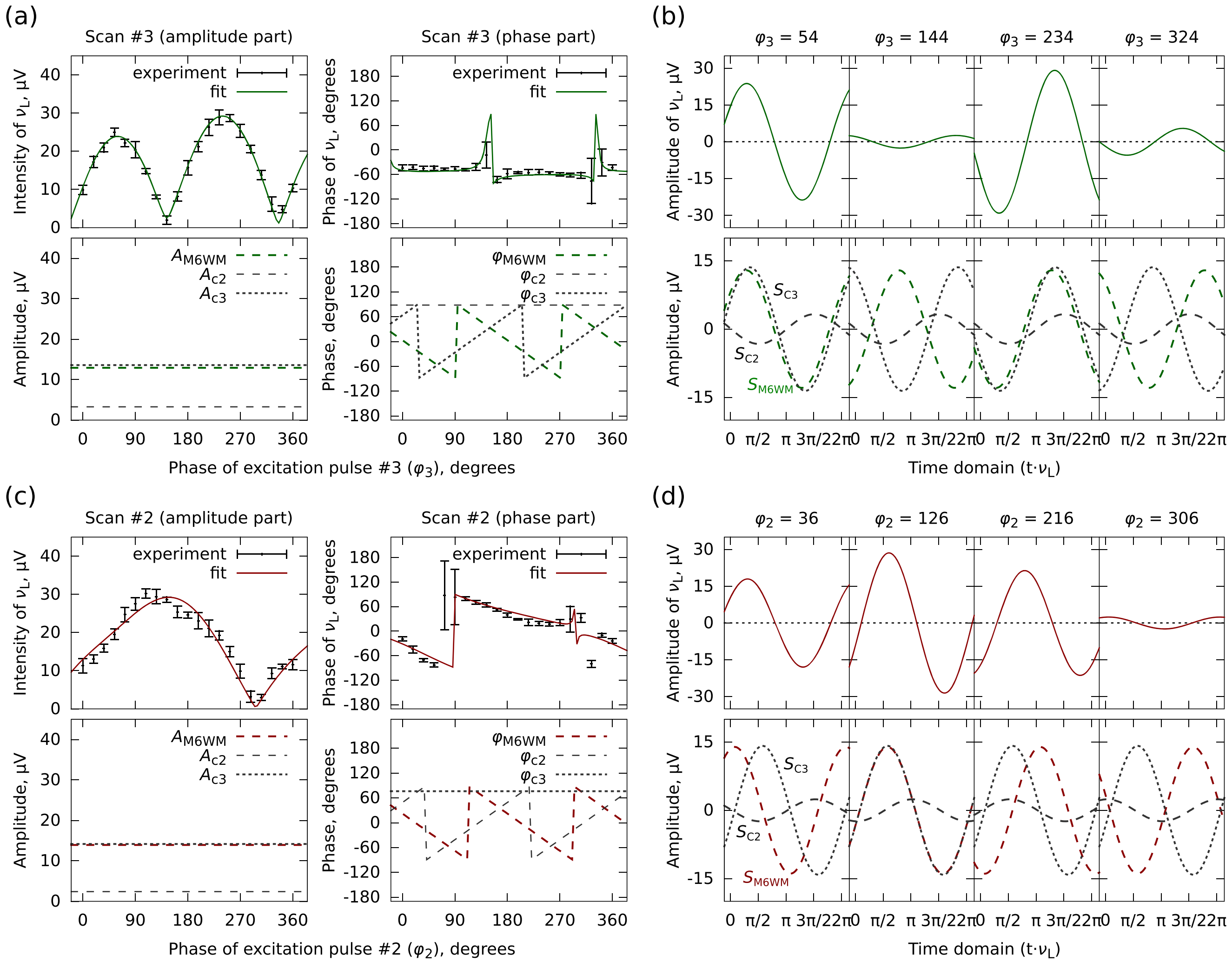

Fig. 4 | Illustration of the interference patterns. Left: experimentally observed interference patterns and the simulations based on the least-squares fits, when scanning the phase of pulse #3 (**a**) and pulse #2 (**c**). The upper traces show the experimental results together with the overall fit with regard to the intensity and phase at the frequency of the listen transition ν_L, respectively. The errors are calculated from a set of five repeated measurements, as mentioned for Fig. 3. The amplitudes and phases of the individual interfering wave components are presented in the lower traces. In each subplot of the phase part, the phase on the y-axis denotes the arctangent of the tangent of the phase. Right: interpretations of the interference in the time domain at four specific phases of φ_3 (**b**) and of φ_2 (**d**). The upper traces in panels **b** and **d** show the total listen signal in the time domain with the observed amplitude and phase, whereas the lower traces exhibit the three time-domain wave components on the basis of the least-squares fit and the experimental pattern. S_{M6WM} (colored dashed line) represents the signal induced from the M6WM scheme. S_{c2} (black dashed lines) and S_{c3} (black dotted lines) are the co-excited signals together with pulses #2 and #3, respectively.

Discussion

By analyzing the observed interference patterns, we have shown that a signal with a non-zero amplitude at the listen transition (ν_L) can be attributed to our phase-controlled M6WM excitation scheme. The amplitude of this signal (S_{M6WM}) is constant (13–14 μV) and the phase of it (φ_{M6WM}) is dependent on the phase φ_k of the k-th pulse with the linear factor s_k. For scans #2 and #3, all three interfering components (S_{M6WM}, S_{c2}, and S_{c3}) are explicitly disentangled, and the fitting results of the two scans show good agreement. As φ_3 or φ_2 is rotated through 360°, the amplitudes of these wave components stay constant, and their phases exhibit different dependencies on φ_3 or φ_2, which are presented in the lower traces of Fig. 4a, c. In scan #3, S_{M6WM} and S_{c3} have similar amplitudes, but their phases rotate with φ_3 in opposite directions. As a result, there are two in-phase and two out-of-phase interference coincidences, as demonstrated with the four time-domain snapshots in Fig. 4b, leading to two maxima/minima in the experimentally observed intensity profile (see Fig. 4a). The two unequal minima and maxima are attributed to the interference with the phase-fixed S_{c2} component. In contrast, in scan #2, the phase of S_{c3} is independent of φ_2, while the phase of S_{M6WM} varies with φ_2. This results in only one in-phase and out-of-phase interference for the S_{M6WM} and S_{c3} signals, one minimum and maximum in the experimental intensity profile, as shown in Fig. 4c and d, respectively. The presence of S_{c2} makes the intensity profile slightly asymmetric.

To understand why the signal S_{M6WM} observed in the experiment is a sign of induced chiral dynamics, we need to compute the *ee* obtained during the pulse sequence. The signed *ee* is an observable that can be expressed via the following operator[16–18]:

$$\hat{ee} = |R\rangle\langle R| - |S\rangle\langle S| = |+\rangle\langle -| + |-\rangle\langle +| . \qquad (3)$$

The pulse sequence and the experiment itself resemble the population transfer experiment followed by a M3WM cycle as a probe of the induced enantiomeric excess as we performed earlier on cyclohexylmethanol (CHM)[12]. For a discussion of the results obtained in the current work, it is useful to compare it with the observations on CHM, where CHM is racemic at room temperature prior to the study, and transient chirality is

Table 1 | Pulse sequence parameters and the fit results of phase scans

Pulse parameters					S_{M6WM}		S_{c2}		S_{c3}	
#	ν, MHz	τ, μs	Ω · τ	Type	s_{M6WM}	A_{M6WM}, μV	s_{c2}	A_{c2}, μV	s_{c3}	A_{c3}, μV
1	9178	0.2	$\frac{\pi}{2}$	c	+1	14	–	–	0	10
2	4373	1.2	π	b	−1	14	+1	2	0	14
3	5293	1.6	π	a	−1	13	0	3	+1	14
4	9231	0.6	π	c	+1	14	–	–	0	11
5	3459	2.0	π	b	−1	13	–	–	0	7

"#" denotes the pulse number for which the phase is being scanned, v is the frequency of the pulse, τ is the pulse duration, and "type" shows the type of the rotational transition excited by the pulse, as well as the direction of the pulse polarization in the laboratory frame. The s are the dimensionless phase dependence coefficients, and the fitted signal amplitudes are denoted by A_{M6WM}, A_{c2}, and A_{c3}, where the subscripts indicate the source of the v_L signal. Details on the fitting procedures are in the Supplementary Information. Note that in scans #1, #4, and #5 the sum of S_{c2} and S_{c3} are fitted, and the corresponding results are shown in the S_{c3} columns.

stabilized in the supersonic jet expansion. The barrier between the enantiomers of CHM is high enough (~15 kJ/mol) to quench the tunneling interconversion of the enantiomers within the time scale of the experiment. Therefore, both the *R* and *S* forms of CHM are present in equal amounts in a gas jet and cannot be converted to each other, leading to |*ee*| = 0 as a starting condition. In the experiments on CHM, we first performed a population transfer for a set of rotational states, creating a non-zero |*ee*| in two particular rotational states. This |*ee*| was then probed by performing an additional M3WM experiment starting from these rotational states.

According to this analogy, in the present study with BA, the first three pulses of the M6WM sequence are analogous to the population transfer part of the experiment, which should induce a non-zero |*ee*| in a specific rotational state. The last two pulses and the induced coherence for the listen transition act as a chiral probe of this enantiomeric enrichment. To elucidate this, one needs to calculate the |*ee*| in the system in the rotational state $|1_{01}\rangle$ after three pulses starting, naturally, with a racemic sample. This quantity is given by the operator $\hat{ee}_{1_{01}} = |1_{01}^+\rangle\langle 1_{01}^-| + |1_{01}^-\rangle\langle 1_{01}^+|$. The explicit calculation (see Supplementary Information for details) shows that after the first three pulses, the resulting state $|\psi\rangle$ will be an oscillating chiral wavepacket, with an amplitude proportional to |*ee*|:

$$\langle\psi|\hat{ee}_{1_{01}}|\psi\rangle \propto \overbrace{\sin(\Omega_1\tau_1)\left(\prod_{k=2}^{3}\sin\left(\frac{\Omega_k\tau_k}{2}\right)\right)}^{\propto\,|ee|}\cdot\sin\left(2\pi\nu_\pm t+\sum_{k=1}^{3}s_k\varphi_k-\Phi'\right). \tag{4}$$

The frequency of the $R \leftrightarrow S$ interconversion is simply a tunneling frequency $\nu_\pm = (E_{1_{01}^-} - E_{1_{01}^+})/h = \epsilon_\pm/h$ (see Fig. 1). Due to the quantum tunneling, the created chiral wavepacket does not have a persistent chirality. However, the polarization induced by the M6WM experiment (Eq. (1)) is proportional to the total magnitude of the |*ee*| induced by the first three pulses. The probed S_{M6WM} with an amplitude of 13–14 μV indicates that a non-zero |*ee*| was created in the rotational state $|1_{01}\rangle$, and the M6WM approach allows us to measure the magnitude of the induced enantiomeric enrichment.

In conclusion, our experiment successfully steered a quantum racemic mixture of two interconvertible enantiomers off-equilibrium in the rotational state of interest by exploiting five microwave radiation pulses from three mutually orthogonal polarizations. This result demonstrates that transient enantiomeric excess can be induced in a quantum tunneling system with a suitable pulse sequence of resonant microwave fields. This provides an approach for manipulating molecular chirality in flexible molecules like BA.

Methods

Sample preparation

The commercial sample of benzyl alcohol (BA) was purchased from Sigma-Aldrich and used without further purification. Experiments were performed using a modified Fourier transform microwave (FTMW) spectrometer in Hamburg, as reported elsewhere[12], and a sketch is provided in Fig. 2. The commercially available sample of BA was placed in an internal sample reservoir close to the solenoid nozzle valve (Parker General Valve, Series 9) and maintained at 70 °C. The sample vapor was seeded by a neon buffer gas with a stagnation pressure of ~3 bar and supersonically expanded into the vacuum chamber via the pulsed valve operating at 6 Hz. The adiabatic expansion efficiently cooled the gas-phase sample to a T_{rot} of ~1–2 K. For each gas pulse, the molecular ensemble was polarized with a series of eight pulse sequences, and 40 μs of FID were recorded following each excitation and averaged on an oscilloscope. After Fourier transformation, the typical frequency resolution of the spectrum is about 25 kHz, giving a full-width at half maximum (FWHM) linewidth of about 60 kHz.

Optimal pulse conditions

To achieve the optimal condition of the proposed M6WM scheme for the population transfer, pulse #1 should be a $\pi/2$-pulse, while the other four pulses (#2 – #5) should be π-pulses. Therefore, nutation curves were performed for each excitation pulse to investigate the evolution of the signal amplitude over the pulse duration in a single-photon excitation experiment. Of them, the power of pulses #1 and #4, #2 and #5, and #3 was amplified to 40 W, 50 W and 3 W, respectively, using solid-state amplifiers (SSA), matching the setup in the subsequent M6WM experiment. The resulting nutation curves are shown in Supplementary Fig. 8, and the obtained optimal durations are summarized in Table 1.

M6WM experiments

To achieve a state-specific enantiomer enrichment, the proposed M6WM experiment was carried out. Using the results of the nutation curves, the five pulses with optimal durations were generated with a two-channel arbitrary waveform generator (AWG), where pulses #1, #3, and #4 are from channel 1 (CH1), and pulses #2 and #5 are from channel 2 (CH2), as illustrated in Fig. 3a. As the polarization direction of pulse #3 needs to be orthogonal to pulses #1 and #4, a single pole double throw (SPDT) pin-diode switch was utilized to feed the signals into the dedicated SSAs. After amplification, the microwave pulses were broadcast into the vacuum chamber to interact with the molecules from three orthogonal polarization directions via two dual-polarization horn antennae. In order to explore the phase dependence of the signal induced from the M6WM scheme, the phase of each signal in the pulse sequence was systematically changed in steps of 18°. The free induction decays (FIDs) of the molecular response were recorded and averaged in the time domain and Fourier transformed into the frequency domain after applying a Gaussian window function. Each phase scan was repeated five times, in which 20,000 FIDs were averaged for each phase point. More details can be found in the Supplementary Information.

Data availability

All the data that support the findings of this study are available within the main text and the Supplementary Information file, and also available from the corresponding author on request.

Code availability

The Python scripts used in this study are provided in the Supplementary Information.

References

1. Nguyen, L. A., He, H. & Pham-Huy, C. Chiral drugs: an overview. *Int. J. Biomed. Sci.* **2**, 85–100 (2006).
2. Beesley, T. E. & Scott, R. P. *Chiral chromatography* (John Wiley & Sons, 1999).
3. Gübitz, G. & Schmid, M. G. Recent progress in chiral separation principles in capillary electrophoresis. *Electrophoresis* **21**, 4112–4135 (2000).
4. Stephens, P. J., Devlin, F. J. & Pan, J. J. The determination of the absolute configurations of chiral molecules using vibrational circular dichroism (VCD) spectroscopy. *Chirality* **20**, 643–663 (2008).
5. Nafie, L. A. *Vibrational optical activity: principles and applications* (John Wiley & Sons, 2011).
6. Lux, C. et al. Circular dichroism in the photoelectron angular distributions of camphor and fenchone from multiphoton ionization with femtosecond laser pulses. *Angew. Chem. Int. Ed.* **51**, 5001–5005 (2012).
7. Garcia, G. A., Nahon, L., Daly, S. & Powis, I. Vibrationally induced inversion of photoelectron forward-backward asymmetry in chiral molecule photoionization by circularly polarized light. *Nat. Commun.* **4**, 2132 (2013).
8. Patterson, D., Schnell, M. & Doyle, J. M. Enantiomer-specific detection of chiral molecules via microwave spectroscopy. *Nature* **497**, 475–477 (2013).
9. Shubert, V. A., Schmitz, D., Patterson, D., Doyle, J. M. & Schnell, M. Identifying enantiomers in mixtures of chiral molecules with broadband microwave spectroscopy. *Angew. Chem. Int. Ed.* **53**, 1152–1155 (2014).
10. Eibenberger, S., Doyle, J. & Patterson, D. Enantiomer-specific state transfer of chiral molecules. *Phys. Rev. Lett.* **118**, 123002 (2017).
11. Pérez, C. et al. Coherent enantiomer-selective population enrichment using tailored microwave fields. *Angew. Chem. Int. Ed.* **56**, 12512–12517 (2017).
12. Pérez, C., Steber, A. L., Krin, A. & Schnell, M. State-specific enrichment of chiral conformers with microwave spectroscopy. *J. Phys. Chem. Lett.* **9**, 4539–4543 (2018).
13. Lee, J. et al. Quantitative study of enantiomer-specific state transfer. *Phys. Rev. Lett.* **128**, 173001 (2022).
14. Quack, M. & Seyfang, G. Chapter 7 - Atomic and molecular tunneling processes in chemistry. In Marquardt, R. & Quack, M. (eds.) *Molecular spectroscopy and quantum dynamics*, 231–282, https://doi.org/10.1016/B978-0-12-817234-6.00012-X (Elsevier, 2021).
15. Ordonez, A. F. & Smirnova, O. Propensity rules in photoelectron circular dichroism in chiral molecules. I. Chiral hydrogen. *Phys. Rev. A* **99**, 043416 (2019).
16. Bychkov, S. S., Grishanin, B. A. & Zadkov, V. N. Laser synthesis of chiral molecules in isotropic racemic media. *J. Exp. Theoretical Phys.* **93**, 24–32 (2001).
17. Bychkov, S. S., Grishanin, B. A., Zadkov, V. N. & Takahashi, H. Laser coherent control of molecular chiral states via entanglement of the rotational and torsional degrees of freedom. *J. Raman Spectrosc.* **33**, 962–973 (2002).
18. Zhdanov, D. V. & Zadkov, V. N. Absolute asymmetric synthesis from an isotropic racemic mixture of chiral molecules with the help of their laser orientation-dependent selection. *J. Chem. Phys.* **127**, 244312 (2007).
19. Hirota, E. Triple resonance for a three-level system of a chiral molecule. *Proc. Jpn Acad. Ser. B* **88**, 120–128 (2012).
20. Hirota, E. Molecular chirality: a new approach from a dynamical point of view. *Proc. Jpn Acad. Ser. B* **93**, 841–849 (2017).
21. Utzat, K. A., Bohn, R. K., Montgomery, J. A., Michels, H. H. & Caminati, W. Rotational spectrum, tunneling motions, and potential barriers of benzyl alcohol. *J. Phys. Chem. A* **114**, 6913–6916 (2010).
22. Domingos, S. R., Pérez, C. & Schnell, M. Sensing chirality with rotational spectroscopy. *Ann. Rev. Phys. Chem.* **69**, 499–519 (2018).
23. Grabow, J.-U. Fourier transform microwave spectroscopy: Handedness caught by rotational coherence. *Angew. Chem. Int. Ed.* **52**, 11698–11700 (2013).
24. Koumarianou, G., Wang, I., Satterthwaite, L. & Patterson, D. Assignment-free chirality detection in unknown samples via microwave three-wave mixing. *Comm. Chem.* **5**, 31 (2022).
25. Rabi, I. I. Space quantization in a gyrating magnetic field. *Phys. Rev.* **51**, 652–654 (1937).
26. Landau, L. D. & Lifshitz, E. M. *Quantum mechanics: non-relativistic theory*, vol. 3 (Elsevier, 2013).
27. Shubert, V. A. et al. Rotational spectroscopy and three-wave mixing of 4-carvomenthenol: a technical guide to measuring chirality in the microwave regime. *J. Chem. Phys.* **142**, 214201 (2015).
28. Leibscher, M., Giesen, T. F. & Koch, C. P. Principles of enantio-selective excitation in three-wave mixing spectroscopy of chiral molecules. *J. Chem. Phys.* **151**, 014302 (2019).
29. Leibscher, M. et al. Full quantum control of enantiomer-selective state transfer in chiral molecules despite degeneracy. *Comm. Phys.* **5**, 110 (2022).
30. Leibscher, M., Kalveram, J. & Koch, C. P. Rational pulse design for enantiomer-selective microwave three-wave mixing. *Symmetry* **14**, https://doi.org/10.3390/sym14050871 (2022).

Acknowledgements

This work has been funded by the Deutsche Forschungsgemeinschaft (DFG, German Research Foundation) - Projektnummer 328961117 - SFB 1319 ELCH. We acknowledge scientific discussions with J.-U. Grabow, T. Giesen, C. Koch, and M. Leibscher. C.P. acknowledges funding from the PID2021-125015NB-I00 grant.

Author contributions

W.S. and D.S.T. contributed equally to this work. C.P. and M.S conceived the project. W.S, H.S, A.L.S, and C.P. performed the experiment. W.S and D.S.T analyzed the data and wrote the paper. All authors contributed to the discussions of the results, and reviewed the manuscript.

Funding

Open Access funding enabled and organized by Projekt DEAL.

Competing interests

The authors declare no competing interests.

Additional information

Supplementary information The online version contains supplementary material available at https://doi.org/10.1038/s41467-023-36653-3.

Correspondence and requests for materials should be addressed to Melanie Schnell.

Peer review information *Nature Communications* thanks the anonymous reviewer(s) for their contribution to the peer review of this work.

Reprints and permissions information is available at http://www.nature.com/reprints

Publisher's note Springer Nature remains neutral with regard to jurisdictional claims in published maps and institutional affiliations.

Open Access This article is licensed under a Creative Commons Attribution 4.0 International License, which permits use, sharing, adaptation, distribution and reproduction in any medium or format, as long as you give appropriate credit to the original author(s) and the source, provide a link to the Creative Commons license, and indicate if changes were made. The images or other third party material in this article are included in the article's Creative Commons license, unless indicated otherwise in a credit line to the material. If material is not included in the article's Creative Commons license and your intended use is not permitted by statutory regulation or exceeds the permitted use, you will need to obtain permission directly from the copyright holder. To view a copy of this license, visit http://creativecommons.org/licenses/by/4.0/.

© The Author(s) 2023